Symbol Timing Recovery for SOQPSK

c2008
Prashanth Chandran

Submitted to the Department of Electrical Engineering &
Computer Science and the Faculty of the Graduate School
of the University of Kansas in partial fulfillment of
the requirements for the degree of Master of Science

Thesis Committee:

Dr. Erik Perrins: Chairperson

Dr. James Roberts

Dr. Shannon Blunt

Date Defended

2008/02/01

The Thesis Committee for Prashanth Chandran certifies
that this is the approved version of the following thesis:

Symbol Timing Recovery for SOQPSK

Committee:

_____

Chairperson

_____

_____

_____

Date Approved

To my sister Sahaana

Acknowledgements

I would like to thank my parents and my sister for all their support and encouragement. You have always been the source of strength and inspiration throughout my life.

I thank my advisor, Dr. Erik Perrins, for his expert advice and guidance, not in just doing this work but throughout my Masters degree at KU. You have helped on numerous occasions in my research without which this work would not have been possible. I also wish to thank Dr. James Roberts and Dr. Shannon Blunt for being in my committee and reviewing this thesis. Your comments were invaluable in preparing this document.

I would also like to thank all my friends who have made my life at KU a happy and memorable one.

Abstract

Shaped offset quadrature phase shift keying (SOQPSK) is a highly bandwidth efficient modulation technique used widely in military and aeronautical telemetry standards. This work focuses on symbol timing recovery for SOQPSK. Continuous phase modulation (CPM) based detector models for SOQPSK have been developed only recently. The proposed timing recovery schemes make use of this recent CPM interpretation of SOQPSK, where SOQPSK is viewed as a CPM with a constrained (correlated) ternary data alphabet. One roadblock standing in the way of these detectors being adopted is that existing symbol timing recovery techniques for CPM are not always applicable since the data symbols are correlated.

Here, we derive timing error detectors (TED) that are extended versions of existing non-data-aided (blind) and data-aided TED's for CPM, where the proposed extensions take the data correlation of SOQPSK explicitly into account. Further, for the nod-data-aided case, the merits of the modified TED are demonstrated by comparing its performance with and *without* taking the data correlation into account. A simple quantization scheme has also been discussed and implemented for the blind TED to yield an extremely low-complexity version of the system with only negligible performance losses. The S-curves of the proposed TED's are given, which rule out the existence of false lock points. Numerical performance results are given for the two versions of SOQPSK: MIL-STD SOQPSK and SOQPSK-TG. These results show that the proposed schemes have great promise in a wide range of applications due to their low complexity, strong performance and lack of false lock points; such applications include timing recovery in noncoherent detection schemes and false lock detectors.

Contents

List of Figures

Chapter 1

Introduction

Shaped-offset quadrature phase shift keying (SOQPSK) is a highly bandwidth efficient form of continuous phase modulation (CPM) [2] based on a constrained (correlated) ternary data alphabet. Its constant-envelope nature makes it transmitter-friendly in terms of its compatibility with non-linear amplifiers and their efficiency in converting limited (e.g. battery) power into radiated power. Power and bandwidth efficiency being the two most important requirements of any modulation scheme, SOQPSK promises to be an attractive candidate for a wide range of applications in various fields.

To date, SOQPSK has been incorporated into military [1] and aeronautical telemetry [18] standards, and wider use is merited since it is applicable in any setting where bandwidth-efficient constant-envelope modulations are needed. Military-standard (MIL-STD) SOQPSK is the original and simplest version; it uses a rectangular shaped frequency pulse that spans a single bit time (full-response) and can be described by a trellis (state machine) with 4 states. A more complicated version has been adopted recently by the aeronautical telemetry group (SOQPSK-TG); this more bandwidth-efficient version has a frequency pulse that spans eight bit times (partial-response) and can be described by a trellis (state machine) with 512 states.

With the increase in demand for such bandwidth and power efficient modulation schemes, it is essential that appropriate receivers are build so as to put them into practial use. One of the most important tasks of a digital communications receiver is synchronization. Carrier, phase and timing are three important parameters whose accurate synchronization is crucial in determining the performance of the digital recever. In this work we primarily deal with symbol timing recovery of one such bandwidth efficient modulation, SOQPSK. The problem of timing synchronization for SOQPSK has been investigated and new synchronization techniques that can be used in *CPM-based* SOQPSK receiver models have been developed.

Two types of timing synchronizers have been developed and explained here. This report is organized in the following manner. In Chap. 2, an overview of the existing detectors for SOQPSK is provided. Further, the need for a CPM based detection scheme is established by comparing the bit error rate performances of the existing and CPM based schemes. In Chap. 3, the mathematical model for the SOQPSK signal is defined followed by a detailed derivation of the performance bound that is to be used in evaluating the timing error detectors (TEDs). Chap. 4 introduces the non-data-aided or the blind TED. This is an adaptation of an existing TED for CPM with some important modifications that have been incorporated so as to make it applicable for SOQPSK. The S-curve for the TED has also been computed to establish the correctness of the scheme. In Chap. 5, the second type of TED is explained. The data-aided TED is derived and applied to the two versions of SOQPSK for two different loop bandwidths. The S-curve of this TED is also computed for both the versions to rule out the possibility of any false lock points. Chap. 6 provides the simulation results for the two schemes. The performance of the two schemes is quantified in terms of normalized timing variance and compared with the modified Cramer-Rao bound (MCRB) as the lower bound on

performance. Bit error curves are also produced for the various cases to compare their performances and explain their accuracy and usefulness. Chap. 7 has the concluding remarks followed by references.

Chapter 2

SOQPSK Detectors

All digital communication systems require some degree of symbol synchronization to the transmitted signals by the receivers. Digital receivers need to be aligned in time to the incoming digital symbol transitions in order to achieve optimum demodulaion. Broadly, these symbol synchronizers can be classified into two categories. The first one assumes that nothing is known about the actual transmitted data sequence. This class is called the non-data-aided (NDA) or blind synchronizers. The other class use the known information about the data stream. This knowledge may be obtained by using the decisions of the receiver, in our case the decisions of the Viterbi algorithm based detector. These are called the data-aided (DA) or decision directed synchronizers.

Talking specifically about SOQPSK detectors, as the name suggests, SOQPSK shares a number of similarities with traditional OQPSK. In fact, until recently, the typical receiver model for SOQPSK has always been a suboptimal OQPSK-type detector and suboptimal OQPSK-type synchronization techniques [8]. Therefore, in the past there has been *no demand* for timing recovery schemes for CPMs with correlated data. However, since CPM-based detectors for SOQPSK have recently been shown to *significantly outperform* OQPSK-based detectors [13] in terms of bit error rate perfor-

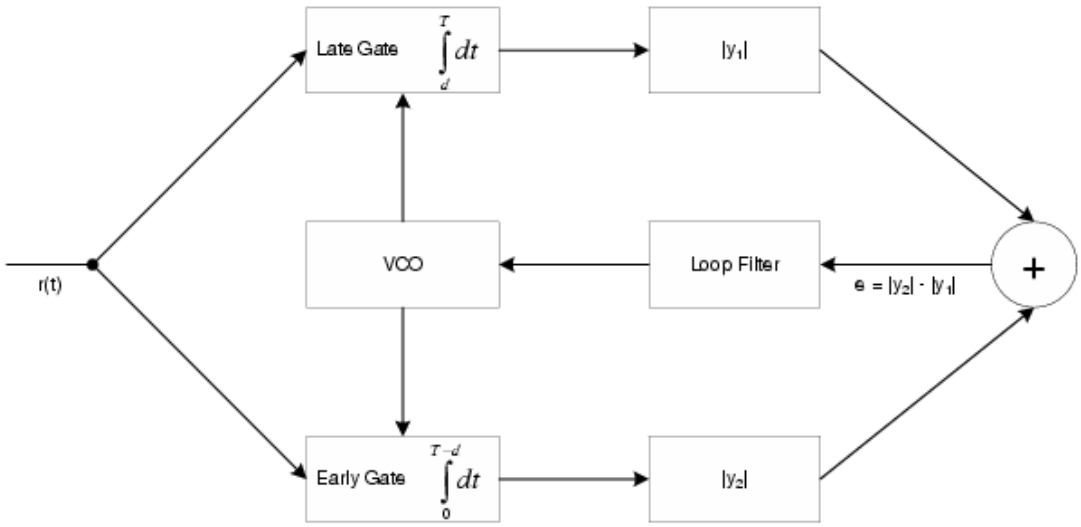

Figure 2.1. Block diagram of the early-late gate synchronization scheme.

mance by 1–2 dB, the motivation is *now present* for synchronization techniques that are compatible with the CPM-based receiver model.

The downside of OQPSK-type detection is that it ignores the inherent state memory of the signal and is not truly *matched* to the transmitted waveform; a performance penalty of 1–2 dB results with symbol-by-symbol OQPSK detection. The shortcomings of OQPSK-type detection have been addressed recently with a cross-correlated trellis quadrature coded modulation (XTCQM) approach in [10] and a CPM-based approach in [15]; both of these recent approaches yield optimal 4-state *trellis-based* detectors for MIL-STD SOQPSK that outperform OQPSK-type detection by 1–2 dB These detectors are optimal in the maximum likelihood sequence detection (MLSD) sense. Furthermore, the CPM-based approach is compatible with powerful CPM complexity reduction techniques, such as the pulse amplitude modulation (PAM) approximation [9, 14] and frequency pulse truncation (PT) technique [3, 21]; these techniques have allowed 4-state detectors for SOQPSK-TG to perform within 0.1 dB of the optimal 512 state detector [16]. Future applications of CPM-based detectors include *noncoherent sequence*

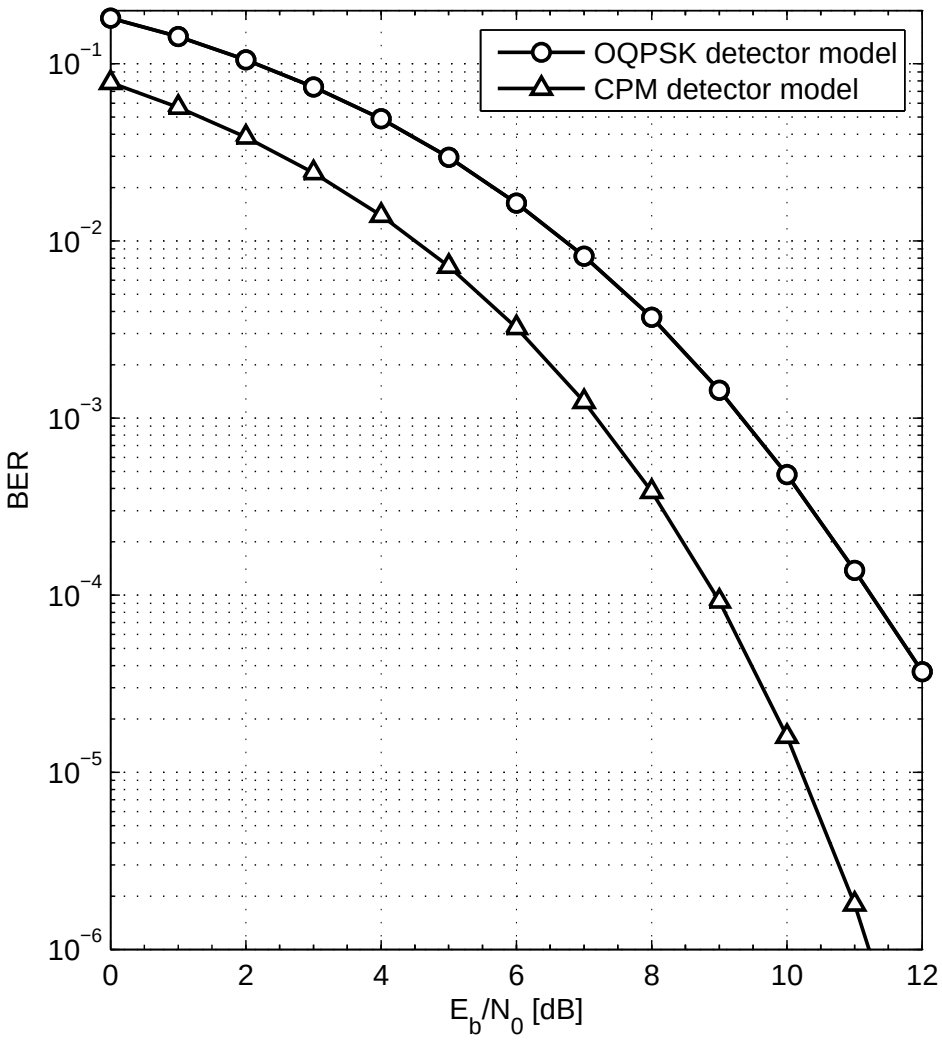

Figure 2.2. Bit error performance of the OQPSK-detector and CPM based detector models for SOQPSK-TG.

detection schemes, e.g. [4], which are of interest for their robustness in operating environments where fully coherent detection is ineffective.

Traditionally, the early-late gate technique shown in Fig. 2.1 is used in the suboptimal synchronization technique. These synchronizers perform two seperate integrations of the incoming signal power, one early and one delayed in time. The difference in output of these two integrations is used to compute the receiver's symbol timing error and is fed back in a loop to correct the error and lock on to the correct time. Though an

early-late gate type synchronizer locks on to the correct timing instant, the 1–2 dB loss incurred by using an OQPSK-type detector cannot be prevented because the matched filters are not correctly matched to the transmitted symbols..

It can be concluded that CPM based detector models yield optimum MLSD detectors, and the 1–2dB performance advantage of CPM-based SOQPSK detection shown in Fig. 2.2 cannot be realized in practice without appropriate synchronization schemes. Thus the synchronization techniques developed here are highly motivated and timely.

Chapter 3

Signal Model

In this chapter we define the mathematical representation of the SOQPSK modulated signal derived from the standard CPM signal. Following this, we define the modified Cramer-Rao bound (MCRB), which is the performance bound used to establish the usefulness of the TEDs and analyze their performances. A detailed discussion of the MCRB is provided explaining the differences in their derivation for two versions of SOQPSK.

3.1 CPM Signal Model

The complex-baseband signal model used to represent CPM signals is defined as [2]

$$s(t, \boldsymbol{\alpha}) \triangleq \sqrt{\frac{E_s}{T_s}} \exp\left\{j\phi(t, \boldsymbol{\alpha})\right\}. \tag{3.1}$$

where E_s is the symbol energy, T_s is the symbol duration and $\phi(\cdot)$ is the phase of the signal. As the name suggests, information in a CPM system is carried in its phase. The

phase $\phi(\cdot)$ is given by

$$\phi(t, \boldsymbol{\alpha}) \triangleq 2\pi h \sum_i \alpha_i q(t - iT_s) \tag{3.2}$$

where $i \in \mathbb{Z}$ is the discrete-time index, α_i is an M-ary symbol, and h is the modulation index. The *phase pulse* $q(t)$ is a time-integral of the *frequency pulse* $g(t)$ and is defined as

$$q(t) \triangleq \begin{cases} 0 & t < 0 \\ \displaystyle\int_0^t g(\sigma)\, d\sigma & 0 \leq t < LT_s \\ 1/2 & t \geq LT_s \end{cases} \tag{3.3}$$

$g(t)$ has a duration of L symbol times with an area of $1/2$. The modulation index h is a rational number of the form [2]

$$h \triangleq \frac{2K}{p}$$

where K and p are relatively prime integers. Considering the modulation index to be a rational number and using the constraints on $g(t)$ and $q(t)$, the phase may be expressed as

$$\phi(t, \boldsymbol{\alpha}) = \theta(t; \boldsymbol{\alpha_n}) + \theta_{n-L}. \tag{3.4}$$

where $nT_s \leq t < (n+1)T_s$. The first term in (3.4) is the *correlative phase* and is defined as

$$\theta(t; \boldsymbol{\alpha_n}) \triangleq 2\pi h \sum_{i=n-L+1}^{n} \alpha_i q(t - iT_s)$$

which is a function of the *correlative state vector*

$$\boldsymbol{\alpha_n} \triangleq \alpha_{n-L+1}, ..., \alpha_{n-1}, \alpha_n.$$

The *phase state* θ_{n-L} in (3.4) is defined as

$$\theta_{n-L} \triangleq \pi h \sum_{i=-\infty}^{n-L} \alpha_i. \tag{3.5}$$

This being a function of an infinite number data symbols can only assume p different values when taken modulo-2π because the modulation index h is assumed to be a rational number. Thus, the p distict values of the *phase state* θ_{n-L} is given by the look-up table

$$\theta[x] = \frac{2\pi x}{p}, \qquad 0 \leq x \leq p-1.$$

Hence, the CPM signal in (3.1) can be described as a finite state machine with input variable α_n and a *correlative* state vector given by

$$S_n = (\theta_{n-L}, \alpha_{n-L+1}, ..., \alpha_{n-2}, \alpha_{n-1}) \tag{3.6}$$

and each branch of the trellis can be defined uniquely as

$$\sigma_n = (\theta_{n-L}, \alpha_{n-L+1}, ..., \alpha_{n-2}, \alpha_{n-1}, \alpha_n). \tag{3.7}$$

The number of states required to describe the CPM signal in (3.1) is [2]

$$N_s = pM^{L-1}.$$

3.2 CPM Model of SOQPSK

The complex-baseband SOQPSK signal model begins with the standard CPM signal defined in (3.1)

$$s(t, \boldsymbol{\alpha}) \triangleq \sqrt{\frac{E_s}{T_s}} \exp\left\{j\phi(t, \boldsymbol{\alpha})\right\}$$

where E_s is the symbol energy and T_s is the symbol duration. In this work, we consider CPM signals where the transmitted symbols $\{\alpha_i\}$ are *not* i.i.d., but are instead *correlated* in some fashion. The data sequence, which we assume to be stationary, has the *autocorrelation function*

$$R_{\boldsymbol{\alpha}}(l) \triangleq \mathrm{E}\left\{\alpha_i \alpha_{i+l}\right\}.$$

The notation used in the derivations herein is *not* specific to SOQPSK and applies to CPM in general. However, numerical results have been provided in Chap. 6 for the two versions of SOQPSK. The original version of SOQPSK, known as "MIL-STD" SOQPSK [1], uses a full-response ($L = 1$) rectangular frequency pulse (1REC). The frequency pulse $g(t)$ for a "MIL-STD" SOQPSK is a rectangular pulse

$$g_{\text{MIL}}(t) \triangleq \begin{cases} \frac{1}{2T}, & 0 \leq t < T_s \\ 0, & \text{otherwise.} \end{cases} \tag{3.8}$$

A version of SOQPSK recently adopted in aeronautical telemetry, known as "SOQPSK-TG," uses the partial response ($L > 1$) frequency pulse shown in Fig. 3.1, which is defined in [18] as

$$g_{\text{TG}}(t) \triangleq A\frac{cos(\frac{\pi\rho Bt}{2T_s})}{1-4(\frac{\rho Bt}{2T_s})^2} \times \frac{sin(\frac{\pi tB}{2T_s})}{\frac{\pi Bt}{2T_s}} \times w(t) \tag{3.9}$$

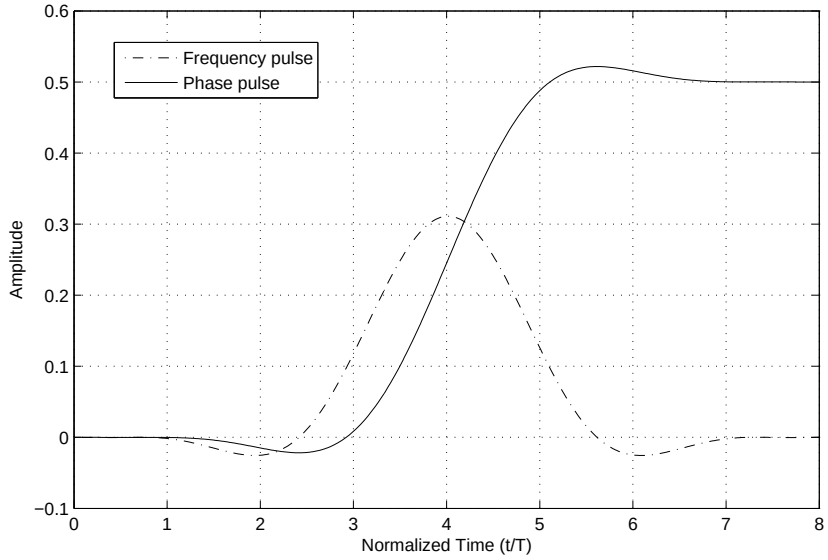

Figure 3.1. Frequency and Phase pulse for SOQPSK-TG

where the window is

$$w(t) = \begin{cases} 1, & 0 \leq \mid \frac{t}{2T_s} \mid < T_{s1} \\ \frac{1}{2} + \frac{1}{2}cos(\frac{\pi}{2}(\frac{t}{2T_s} - T_{s1})), & T_{s1} \leq \mid \frac{t}{2T_s} \mid \leq T_{s1} + T_{s2} \\ 0, & T_{s1} + T_{s2} < \mid \frac{t}{2T_s} \mid \end{cases} \tag{3.10}$$

The constant A is chosen such that the area of the pulse is $1/2$ with $T_{s1} = 1.5$, $T_{s2} = 0.5$, $\rho = 0.7$ and $B = 1.25$.

The modulation index for all versions of SOQPSK is $h = 1/2$ and the transmitted symbols $\{\alpha_i\}$ are derived from a sequence of i.i.d. information symbols $\{u_i\}$ by a *precoding* operation [19]

$$\alpha_i(\boldsymbol{u}) \triangleq (1/2)(-1)^{i+1}u_{i-1}(u_i - u_{i-2}) \tag{3.11}$$

where $u_i \in \{\pm 1\}$ and $\alpha_i \in \{-1, 0, +1\}$. The reason for this non-obvious precoding operation is that (3.11) orients the phase of the CPM signal in (3.2) such that it behaves like the phase of an OQPSK signal that is driven by the i.i.d. bit sequence $\boldsymbol{u}$. In fact, $\boldsymbol{u}$ can be recovered directly from the received signal, with no additional steps, by a suboptimal symbol-by-symbol OQPSK-type detector [7, 8]. For convenience, we use the notation α_i instead of $\alpha_i(\boldsymbol{u})$, but we stress that $\boldsymbol{u}$ is the underlying information sequence for SOQPSK.

The SOQPSK precoder imposes three important constraints on the ternary data [19]:

1. While α_i is viewed as being *ternary*, in any given bit interval α_i is actually drawn from one of two *binary* alphabets, $\{0, +1\}$ or $\{0, -1\}$.

2. When $\alpha_i = 0$, the binary alphabet for α_{i+1} switches from the one used for α_i, when $\alpha_i \neq 0$ the binary alphabet for α_{i+1} does not change.

3. A value of $\alpha_i = +1$ cannot be followed by $\alpha_{i+1} = -1$, and vice versa (this is implied by the previous constraint).

Based on these constraints, the autocorrelation function for SOQPSK is [20]

$$R_{\boldsymbol{\alpha}}(l) = \begin{cases} 1/2, & l = 0 \\ 1/4, & |l| = 1 \\ 0 & \text{otherwise.} \end{cases} \tag{3.12}$$

The above constraints also imply that not every possible ternary symbol pattern is a valid SOQPSK data pattern. For example, the ternary symbol sequences ..., $0, +1, -1, 0, ...$ and $\ldots, +1, 0, +1, \ldots$ violate the SOQPSK constraints. Therefore, if we consider the entire set of $3^{\Delta K}$ possible ternary symbol sequences of length-ΔK, it has been shown

that only

$$N_{\Delta K} \triangleq 2^{\Delta K+1} \tag{3.13}$$

of these are valid SOQPSK data patterns [17]. A straightforward method of generating this entire set of sequences is to start with a binary $(\Delta K + 1)$-tuple $(S, \boldsymbol{u})$, where the value of S is used to initialize the value of i in (3.11) (this initializes the "alphabet state" of the precoder to $\{0, +1\}$ or $\{0, -1\}$), and $\boldsymbol{u}$ is a sequence of ΔK binary symbols. The other initial conditions in (3.11), u_{i-1} and u_{i-2}, can both be initialized to $+1$. The set of $N_{\Delta K}$ valid SOQPSK data patterns is generated by running all possible permutations of $(S, \boldsymbol{u})$ through the precoder in (3.11).

3.3 Performance Bounds

We use the modified Cramer-Rao bound (MCRB) [6] to establish a lower bound on the degree of accuracy to which τ can be estimated for CPMs with correlated data. If we define λ as an element that is to be estimated, and let $\hat{\lambda}(\boldsymbol{r})$ be the corresponding estimate, then $\hat{\lambda}(\boldsymbol{r})$ depends on the obseravtion $\boldsymbol{r}$. In other words, $\hat{\lambda}(r)$ is a random variable. Its expectation may, or may not, coincide with the true value of λ. If it does, then the estimate is said to be *unbiased* and the estimator is called an *unbiased estimator*. However, the performance of the estimator can be unsatisfactory if the errors $\hat{\lambda}(\boldsymbol{r}) - \lambda$ are widely scattered around zero.

3.3.1 Definition of Cramer-Rao Bound

The Cramer-Rao bound (CRB) gives us the lower bound to the variance of any unbiased estimator. Defining λ as the single element that is to be estimated, and representing

all other parameters as **v**, the bound is expressed as [11]

$$\text{Var}\left\{\hat{\lambda}(\boldsymbol{r}) - \lambda\right\} \geq \text{CRB}(\lambda) \tag{3.14}$$

where $\text{CRB}(\lambda)$ is given by [6]

$$\text{CRB}(\lambda) = \frac{1}{\text{E}_{\mathbf{r}}\left\{\left[\frac{\partial \ln p(\boldsymbol{r}|\lambda)}{\partial \lambda}\right]^2\right\}} \tag{3.15}$$

where $\text{E}_{\mathbf{r}}$ is the expectation with respect to $\boldsymbol{r}$ and $p(\boldsymbol{r} \mid \lambda)$ is the conditional probability density function of $\boldsymbol{r}$ for a given λ. $p(\boldsymbol{r} \mid \lambda)$ is obtained from the integral [6]

$$p(\boldsymbol{r} \mid \lambda) = \int_{-\infty}^{\infty} p(\boldsymbol{r} \mid \mathbf{v}, \lambda) p(\mathbf{v}) d\mathbf{v} \tag{3.16}$$

where $p(\boldsymbol{r} \mid \mathbf{v}, \lambda)$ is the conditional probability density function of **r** given **v** and λ. Unfortunately, in most practical cases it is difficult to compute the CRB because the integration in (3.16) is analytically complex or the expectation in (3.15) poses problems. A simpler bound to compute is the MCRB which is used as the theoretical performance bound in this work. The relationship between the MCRB and CRB is given by [11]

$$\text{CRB}(\lambda) \geq \text{MCRB}(\lambda). \tag{3.17}$$

This equality holds good when **v** is *perfectly* known or it is *empty* (there are no unwanted parameters).

3.3.2 Modified Cramer-Rao Bound

As discussed in Sec. 3.3.1, the CRB uses the maximum likelihood function to establish the lower bound. The MCRB is determined using the transmitted signal and is much easier to compute. Defining θ as the phase offset, ν as the carrier frequency offset and following the approach in [11, Ch. 2], we separate the timing offset τ from the set of other parameters, $\mathbf{v} = \{\boldsymbol{\alpha}, \theta, \nu\}$, that are unwanted in the timing estimation problem. The complete complex-baseband signal model can be written using (3.2) as

$$s(t, \tau, \mathbf{v}) \triangleq \sqrt{\frac{E_s}{T_s}} e^{j[\phi(t-\tau, \boldsymbol{\alpha}) + 2\pi\nu t + \theta]}. \tag{3.18}$$

The MCRB with respect to τ for a baseband signal is [11]

$$\text{MCRB}(\tau) \triangleq \frac{N_0/2}{\text{E}_{\mathbf{v}} \left\{ \int_0^{T_0} \left| \frac{\partial s(t, \tau, \mathbf{v})}{\partial \tau} \right|^2 dt \right\}} \tag{3.19}$$

where $T_0 \triangleq L_0 T_s$. Next, using the signal model in (3.18), we get

$$\text{E}_{\boldsymbol{\alpha}} \left\{ \int_0^{T_0} \left| \frac{\partial s(t; \boldsymbol{\alpha}, \tau)}{\partial \tau} \right|^2 dt \right\} = \frac{4\pi^2 h^2 L_0 C_g E_s}{T_s^2}$$

where the constant

$$C_g \triangleq T_s \int_0^{T_s} G(t, \tau)\, dt \tag{3.20}$$

is a function of the frequency pulse $g(t)$. The integrand in (3.20) is periodic in t with period T_s and is defined as

$$G(t,\tau) \triangleq \mathrm{E}_{\boldsymbol{\alpha}}\left\{\left|\sum_i \alpha_i g(t-iT_s-\tau)\right|^2\right\} \tag{3.21}$$
$$= \sum_i \sum_l R_{\boldsymbol{\alpha}}(l) g(t-iT_s-\tau) g(t-[i+l]T_s-\tau)$$

and $R_{\boldsymbol{\alpha}}(l)$ is the autocorrelation function of the sequence $\boldsymbol{\alpha}$.

At this point, the solution can be expressed in closed-form for MIL-STD SOQPSK using (3.12). In this case, (3.21) simplifies to

$$G_{\text{MIL}}(t,\tau) = \frac{1}{2}\sum_i g_{\text{MIL}}^2(t-iT_s-\tau) = \frac{1}{8T_s^2} \tag{3.22}$$

where only the $l=0$ term is non-zero due to the brief duration of $g_{\text{MIL}}(t)$ (full-response, $L=1$). Evaluating (3.22) yields $G_{\text{MIL}}(t,\tau) = 1/8$, using which the final result for MIL-STD SOQPSK is

$$\frac{1}{T_s^2} \times \text{MCRB}_{\text{MIL}}(\tau) = \frac{4}{\pi^2 L_0} \times \frac{1}{E_s/N_0}. \tag{3.23}$$

For SOQPSK-TG, a similar closed-form equation is difficult to compute due to the shape of $g_{\text{TG}}(t)$ which is a custom-designed partial-response pulse with $L=8$. But, (3.21) can be computed numerically with ease. Using (3.12) it is seen that only the $l=0$ and $l=\pm 1$ terms will be non-zero as the correlation is zero for $l>1$. Hence, for SOQPSK-TG (3.21) can be simplified as

$$\begin{aligned} G_{\text{TG}}(t,\tau) = &\frac{1}{2}\sum_i g_{\text{TG}}^2(t-iT_s-\tau) \\ &+ \frac{1}{2}\sum_i g_{\text{TG}}(t-iT_s-\tau) g_{\text{TG}}(t-(i+1)T_s-\tau) \end{aligned} \tag{3.24}$$

Evaluating (3.24) numerically yields the final result for SOQPSK-TG as

$$\frac{1}{T_s^2} \times \text{MCRB}_{\text{TG}}(\tau) = \frac{1}{2\pi^2 L_0 C_{\text{TG}}} \times \frac{1}{E_s/N_0} \tag{3.25}$$

where $C_{\text{TG}} \approx 0.09881$.

Chapter 4

Non Data Aided TED

A typical assumption in most communication systems is that the transmitted data are *independent* and *identically distributed*, or i.i.d. However, for one reason or another, this is not always the case. SOQPSK is an example of such a case with correlated data symbols.

The problem of symbol timing recovery for CPMs with correlated data has not been studied previously. There are at least two reasons for this: 1) the only obvious example of such a CPM is SOQPSK, and 2) as explained earlier in Chap. 2, CPM-based *transmitter* models have always been used for SOQPSK, but it is only recently that optimal CPM-based *receiver* models have been used for SOQPSK, e.g. [15].

The contributions in this chapter of the work are the following:

- Develop a maximum-likelihood-based non-data-aided (blind) timing error detector (TED) for CPMs with correlated data symbols. The proposed TED is an extension of the one developed in [5] for CPMs with i.i.d. data.

- Develop a quantization scheme for the TED that yields a low-complexity version of the system with only negligible performance losses. This quantization scheme

is not limited to CPMs with correlated data and can be applied to conventional CPMs, i.e. [5].

- Compare the performance of the TED with and *without* taking the data correlation into account.

- Evaluate the correctness of the TED by computing the S-curve and thereby establishing the absence of any false lock points.

Although "MIL-STD" SOQPSK [1] is used as the default example, the TED is derived using general notation and is not specific to this special case. Since the proposed scheme is shown to have low complexity, no false lock points, and a blind architecture, it is an attractive candidate for a wide range of applications. One such application is timing recovery for noncoherent detection schemes, where *joint* timing and phase recovery approaches are not practical since the phase of the signal is never recovered.

This chapter is organized as follows. Section 4.1 shows the extensions that are needed for the existing TED, and also discusses the quantization scheme and the original formulation of the TED that ignores the correlation in the data. Section 4.2 presents the S-curve of the proposed TED. The performance analysis of this TED is provided in Section 6.1 which contains the numerical results.

4.1 Timing Error Detector

The derivation of the timing error detector (TED) starts and ends in similar places as [5]; however, an important part in the middle of the derivation is different due to the correlated data symbols instead of i.i.d. data.

The signal observed at the receiver is

$$r(t) = \sqrt{\frac{E_s}{T_s}} e^{j[\phi(t-\tau,\boldsymbol{\alpha})+2\pi\nu t+\theta]} + w(t)$$

where $w(t)$ is complex-valued additive white Gaussian noise (AWGN) with zero mean and single-sided power spectral density N_0. The frequency offset, ν, is assumed to be known at the receiver. The variables $\boldsymbol{\alpha}$, θ, and τ represent the data symbols, carrier phase, and timing offset, respectively, which are all assumed to be unknown at the receiver.

Denoting $0 \leq t \leq L_0 T$ as the observation interval, the joint likelihood function for $\tilde{\boldsymbol{\alpha}}$, $\tilde{\theta}$, and $\tilde{\tau}$ is given in [5] as

$$\Lambda(\boldsymbol{r}|\tilde{\boldsymbol{\alpha}}, \tilde{\theta}, \tilde{\tau}) = e^{\frac{1}{N_0}\sqrt{\frac{E_s}{T_s}}\mathrm{Re}\left[e^{-j\tilde{\theta}} \int_0^{L_0 T_s} r(t) e^{-j[2\pi\nu t+\phi(t-\tilde{\tau},\tilde{\boldsymbol{\alpha}})]} dt\right]}.$$

Averaging this expression over the carrier phase $\tilde{\theta}$, taking $\tilde{\theta}$ to be uniformly distributed over $[0, 2\pi)$ results in an intermediate likelihood function, which is found in [5] and is a function of $\tilde{\boldsymbol{\alpha}}$ and $\tilde{\tau}$. This intermediate likelihood function is then averaged over $\tilde{\boldsymbol{\alpha}}$ to yield [5]

$$\Lambda(\boldsymbol{r}|\tilde{\boldsymbol{\tau}}) \approx \int_0^{L_0 T_s} \int_0^{L_0 T_s} r(t_1) r^*(t_2) e^{j2\pi\nu(t_2-t_1)} F(t_2-t_1, t_2-\tilde{\tau}) dt_1 dt_2 \tag{4.1}$$

where $F(\Delta t, t)$ contains the expectation over $\tilde{\boldsymbol{\alpha}}$ and is defined as

$$F(\Delta t, t) \triangleq \mathrm{E}_{\tilde{\boldsymbol{\alpha}}} \left\{ e^{j[\phi(t,\tilde{\boldsymbol{\alpha}})-\phi(t-\Delta t,\tilde{\boldsymbol{\alpha}})]} \right\}. \tag{4.2}$$

Using (3.2) we can write (4.2) as

$$F(\Delta t, t) = \mathrm{E}_{\tilde{\boldsymbol{\alpha}}} \left\{ \prod_{i=-\infty}^{\infty} \exp\left[j2\pi h \tilde{\alpha}_i p(t - iT_s, \Delta t) \right] \right\} \tag{4.3}$$

where

$$p(t, \Delta t) \triangleq q(t) - q(t - \Delta t).$$

Evaluating (4.3) is straightforward for i.i.d. data, since the expectation operator can be moved inside the product where it is a function of only one symbol, $\tilde{\alpha}_i$, and can be computed with ease (see [5]). However, another option must be pursued here since the data symbols are assumed to be correlated. This is where the present derivation differs from that found in [5].

4.1.1 Evaluating the Expectation With Respect to $\tilde{\boldsymbol{\alpha}}$

We start by exploiting the fact that $p(t, \Delta t)$ is non-zero for only a few values of i [this is due to the definition of the phase pulse in (3.3)]. The limits on the product in (4.3) can be written as

$$F(\Delta t, t) = \mathrm{E}_{\tilde{\boldsymbol{\alpha}}} \left\{ \prod_{i=K_1}^{K_2} \exp\left[j2\pi h \tilde{\alpha}_i p(t - iT_s, \Delta t) \right] \right\} \tag{4.4}$$

where

$$K_1 = \left\lfloor \frac{\min(t, t - \Delta t)}{T_s} \right\rfloor - L + 1$$

and

$$K_2 = \left\lfloor \frac{\max(t, t - \Delta t)}{T_s} \right\rfloor$$

with $\lfloor \cdot \rfloor$ denoting the floor function. Therefore, the data sequence $\{\tilde{\alpha}_i\}$ in (4.4) has a finite length of $\Delta K \triangleq K_2 - K_1 + 1$ symbols. The problem of evaluating the expec-

tation in (4.4) reduces to 1) enumerating the possible length-ΔK $\tilde{\boldsymbol{\alpha}}$ sequences and 2) attaching a probability distribution to these sequences.

In the case of SOQPSK, the number of possible length-ΔK $\tilde{\boldsymbol{\alpha}}$ sequences is enumerated in (3.13) and the binary $(\Delta K+1)$-tuples $(\tilde{S}, \tilde{\boldsymbol{u}})$ that produce them are independent and uniformly distributed.[1] Therefore, the expectation in (4.4) can be taken with respect to the uniformly distributed variable $(\tilde{S}, \tilde{\boldsymbol{u}})$, i.e.

$$F(\Delta t, t) = \frac{1}{N_{\Delta K}} \sum_{(\tilde{S}, \tilde{\boldsymbol{u}})} \prod_{i=K_1}^{K_2} \exp\Big[j2\pi h \tilde{\alpha}_i(\tilde{S}, \tilde{\boldsymbol{u}}) p(t - iT_s, \Delta t) \Big] \tag{4.5}$$

where the ternary symbols $\tilde{\alpha}_i(\tilde{S}, \tilde{\boldsymbol{u}})$ are explicitly shown to be a function of $(\tilde{S}, \tilde{\boldsymbol{u}})$. It is straightforward to evaluate (4.5) numerically. In fact, numerical computations are already a part of the final derivation in [5] of the TED.

4.1.2 Final Derivation of the TED

The final steps in deriving the TED are the same as found in [5]. The ultimate goal is to compute the argument $\tilde{\tau}$ which maximizes $\Lambda(\boldsymbol{r}|\tilde{\boldsymbol{\tau}})$ in (4.1). To achieve this we must simplify (4.1) due to the cumbersome form of $F(\Delta t, t)$; this function, even in its new form in (4.5), is periodic with respect to t of period T. Therefore, its Fourier series expansion is exploited in evaluating (4.1). The final form of Fourier series expansion of the likelihood function in (4.1), after exploiting various symmetries, is [5].

$$\Lambda(\boldsymbol{r}|\tilde{\boldsymbol{\tau}}) \approx \text{Re}\left[\sum_{m=1}^{\infty} A(m) e^{j2\pi m \tilde{\tau}/T_s} \right] \tag{4.6}$$

[1] There are actually two values of $(\tilde{S}, \tilde{\boldsymbol{u}})$ that produce the all-zeros $\tilde{\boldsymbol{\alpha}}$ sequence. Thus, strictly speaking, there is not a one-to-one mapping between $(\tilde{S}, \tilde{\boldsymbol{u}})$ and $\tilde{\boldsymbol{\alpha}}$. However, it is true that the underlying behavior of the precoder is correctly characterized by the uniformly distributed random variable $(\tilde{S}, \tilde{\boldsymbol{u}})$, which means that the all-zeros $\tilde{\boldsymbol{\alpha}}$ should appear twice in the expectation.

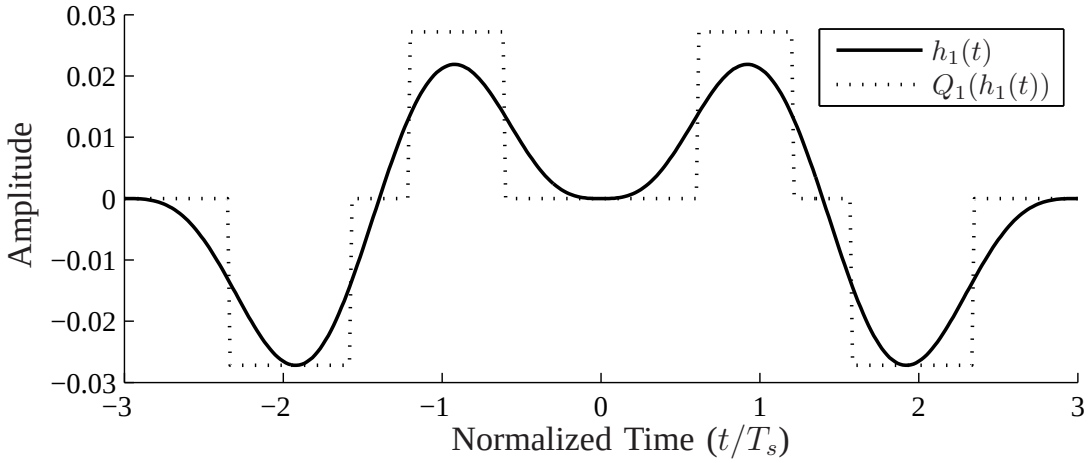

Figure 4.1. The impulse response $h_1(t)$ for MIL-STD SOQPSK.

with

$$A(m) = \int_0^{L_0 T_s} \left[r(t) e^{-j\pi m t/T_s} \right] y_m^*(t)\, dt$$

where

$$y_m(t) \triangleq \int_0^{L_0 T_s} \left[r(\sigma) e^{j\pi m \sigma/T_s} \right] h_m(t-\sigma)\, d\sigma$$

and

$$h_m(t) \triangleq e^{j\pi m t/T_s} \frac{1}{T_s} \int_0^{T_s} F(-t,u) e^{j2\pi m u/T_s} du. \tag{4.7}$$

The pulse $h_1(t)$, which is computed using $F(\Delta t, t)$ in (4.5), is shown in Fig. 4.1 for MIL-STD SOQPSK. The trend observed here, which is the same as that observed in [5], is that the energy in the pulses $h_m(t)$ decreases rapidly as the Fourier series harmonic index m increases. Therefore, the likelihood function in (4.6) is well approximated by the single term where $m = 1$.

A discrete-time implementation of (4.6) using the $m = 1$ term only is shown in block diagram form in Fig. 4.2. The impulse response of the filter is sampled at N samples per symbol to yield

$$h[k] \triangleq h(kT)$$

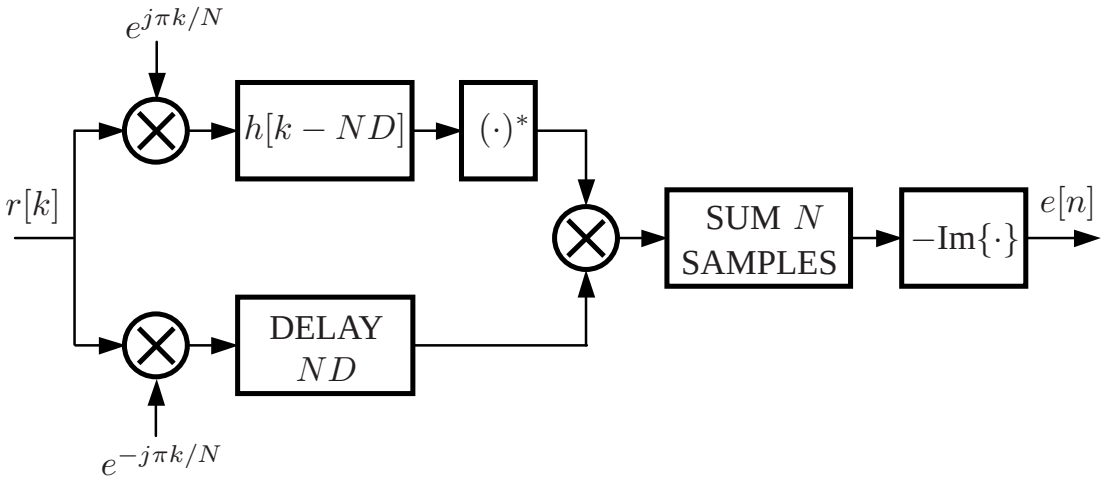

Figure 4.2. Block diagram of the final TED.

where $T \triangleq T_s/N$ is the sampling time. The subscript on this impulse response has been dropped in Fig. 4.2, for reasons that will become clear momentarily; however, at this point it is understood that $h[k] = h_1[k]$. The impulse response of the filter is the only part of the system in Fig. 4.2 that is specific to the modulation format. The block diagram in Fig. 4.2 shows that the non-causal impulse response $h[k]$ is made causal by introducing an appropriate delay of ND samples.

4.1.3 Quantization of $h_1(t)$

Although the system in Fig. 4.2 does not require an unreasonable amount of implementation complexity, most of its complexity is due to computing the N filter outputs. With the most efficient discrete-time implementation, these filter outputs require

$$2N\left(\frac{L_{h[k]}-1}{2}+1\right)$$

multiplications per symbol time, where $L_{h[k]}$ is the number of non-zero samples in $h[k]$. For MIL-STD SOQPSK with $N = 4$, this comes to 104 multiplications per symbol

time.

In an effort to reduce the complexity of the TED while maintaining its performance, we explore the idea of quantizing the values of $h_1(t)$. One possible quantization scheme is

$$Q_l(x(t)) = \text{round}\left(\frac{x(t)2^{l-1}}{M_x}\right)\frac{M_x}{2^{l-1}}, \qquad l > 0 \tag{4.8}$$

where round$(\cdot)$ denotes "round towards the nearest integer" and

$$M_x = \max_t(|x(t)|). \tag{4.9}$$

The parameter l denotes that $l+1$ bits are used to quantize the input signal $x(t)$, where l bits quantize the amplitude and one bit is used as the sign bit. While (4.8) and (4.9) use continuous-time notation, they are equally applicable to a discrete-time input of $x[k]$.

The most extreme example of this quantization scheme is with $l = 1$. The shape of $Q_1(h_1(t))$ for MIL-STD SOQPSK is shown in Fig. 4.1. No multiplications are required to compute the output of the filter in Fig. 4.2 when $h[k] = Q_1(h_1[k])$. The performance of the TED with $h[k] = Q_1(h_1[k])$ is quantified for the case of MIL-STD SOQPSK in Section 6.1.

4.1.4 Generating $h_1(t)$ When the Correlation is Ignored

We have shown how to evaluate the expectation in (4.2) when the data sequence $\tilde{\boldsymbol{\alpha}}$ is correlated. However, it is reasonable to wonder whether or not the re-derivation of $h_1(t)$ is even necessary. In other words, how well would the TED in Fig. 4.2 perform if the data correlation is ignored when $h_1(t)$ is computed? The answer to such a question depends, of course, on the degree of correlation in $\tilde{\boldsymbol{\alpha}}$. Thus, while a general answer cannot be given, the question is worth considering for our example case of MIL-STD SOQPSK.

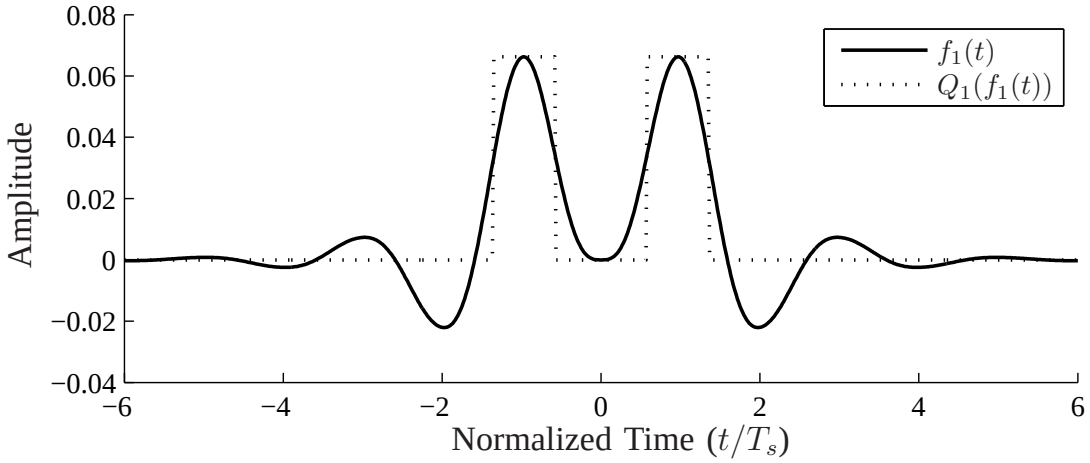

Figure 4.3. The impulse response $f_1(t)$ for MIL-STD SOQPSK.

In order to keep things separate, we use $f_1(t)$ to refer to the pulse obtained from (4.7) with $m = 1$ when *uncorrelated* (i.i.d) data are assumed. In the case of SOQPSK, an unconstrained ternary alphabet has $N_{\Delta K} = 3^{\Delta K}$ unique sequences of length-ΔK. This set of i.i.d. sequences can be used to evaluate (4.5), or the original formulation of $F(\Delta t, t)$ in [5] can be used. The resulting pulse $f_1(t)$, and its quantized version $Q_1(f_1(t))$, are shown in Fig. 4.3 for MIL-STD SOQPSK. Between Figs. 4.1 and 4.3 there are four options for the filter response $h[k]$ in the TED in Fig. 4.2. Numerical results on the individual performances of these four filter options are given in Section 6.1.

4.2 S-curve of the TED

The behavior of the TED is characterized by the S-curve, which is the expected value of the TED output $e[n]$ as a function of the *timing offset*

$$\delta \triangleq \tau - \hat{\tau}.$$

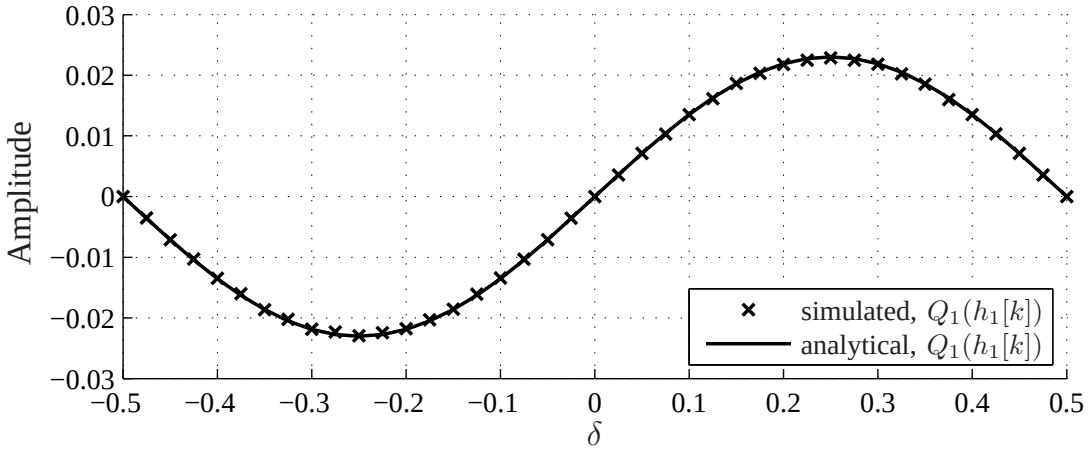

Figure 4.4. S-curve for MIL-STD SOQPSK with $h[k] = Q_1(h_1[k])$ and $N = 4$.

The S-curve is particularly useful since it identifies the stable lock points for the TED and proves the correctness of the TED ruling out possibility of false lock points. Stable lock points are the zero-crossing points on the curve where the slope is positive, e.g. [11].

The S-curve for the TED in Fig. 4.2 was computed in [12] assuming the original and exact impulse response is used, i.e. assuming $h[k] = h_1[k]$. The resulting S-curve is

$$S(\delta) = \frac{E_s N H}{T} \sin\left(\frac{2\pi\delta}{T}\right). \tag{4.10}$$

When a generic impulse response $h[k]$ is used, the S-curve is also given by (4.10), with the definition of H altered slightly from [12], i.e.

$$H \triangleq \sum_k h_1[k]h[k]. \tag{4.11}$$

Thus, a quantized (or otherwise non-exact) impulse response $h[k]$ changes only the *amplitude* of the S-curve, and not its *shape*. When the original and exact impulse response is used, (4.11) reduces to the expression defined in [12].

The S-curve in (4.10) is shown in Fig. 4.4 for MIL-STD SOQPSK with $h[k] = Q_1(h_1[k])$ and $N = 4$, along with data points taken from computer simulations. The simulation points in Fig. 4.4 show strong agreement with the theoretical S-curve, which underscores the correctness of (4.11). Also, as (4.10) and Fig. 4.4 suggest, only one stable lock point exists for the TED in Fig. 4.2; this point occurs when the timing estimate is correct, i.e. at $\delta = 0$, which rules out the existence of any false lock points.

Chapter 5

Data Aided TED

The second option available for timing synchronization is the data aided TED. As in the previous case, we can use an existing TED for CPM and make the necessary modifications to suit our needs of SOQPSK. The specific contributions of this chapter are the following:

- Adapt an existing CPM-based timing error detector (TED) [12] so that the constrained ternary nature of CPM is properly taken into account.
- Incorporate the TED into the Viterbi algorithm (VA) based SOQPSK detectors and properly combine it with the 4-state pulse-truncation (PT) technique.
- Evaluate the correctness of the TED by computing the S-curve and thereby establishing the absence of any false lock points.

This scheme as we will see shortly has low complexity, low normalized variance that approaches the MCRB, and is free of false lock points.

This chapter is organized as follows. In Section 5.1 we derive the TED using maximum-likelihood methods and making some minor modifications to the existing

one. In 5.2, we compute the S-curve and establish the absence of any false lock points. The lower bound on the performance of the proposed approach has already been established in Section 3.3 by computing the MCRB and the numerical results for the data-aided TED are provided in Section 6.2.

5.1 Timing Error Detector

The derivation of the timing error detector (TED) is based on maximum likelihood principles. The signal observed at the receiver is modeled as

$$r(t) = \sqrt{\frac{E_s}{T_s}} e^{j\phi(t-\tau,\boldsymbol{\alpha})} + w(t)$$

where $w(t)$ is complex-valued additive white Gaussian noise (AWGN) with zero mean and single-sided power spectral density N_0. The variables $\boldsymbol{\alpha}$ and τ represent the data symbols and timing offset, respectively, which are both unknown to the receiver in practice.

The operation of the TED is intertwined with the operation of the Viterbi algorithm (VA). Customarily, CPM signals are demodulated using a bank of M^L matched filers (MFs). But, in the case of SOQPSK it is important to note that though the original underlying data is binary, the precoding operation produces a ternary output and hence the MF bank for full-response SOQPSK is made of an array of three filters matched to $\{-1, 0, 1\}$. By applying the PT approximation [3, 21], it was shown in [16] that the same three MFs can be used for partial-response SOQPSK-TG.

Recall the equation from Chap. 3, the phase of a CPM signal is given by

$$\phi(t, \boldsymbol{\alpha}) \triangleq 2\pi h \sum_i \alpha_i q(t - iT_s).$$

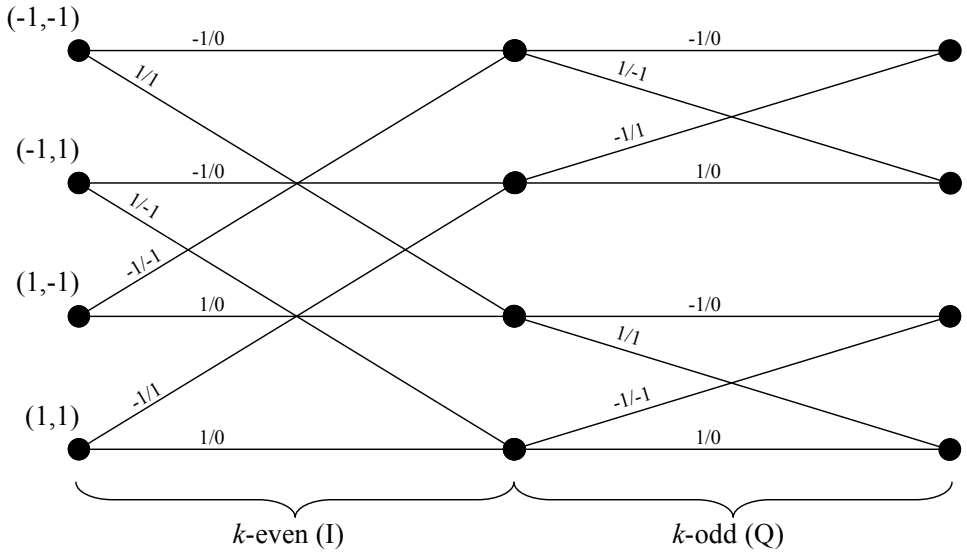

Figure 5.1. Four state trellis diagram for SOQPSK.

This equation can be rewritten in the following form

$$\phi(t, \boldsymbol{\alpha}) = \eta(t, \boldsymbol{C}_k, \alpha_k) + \boldsymbol{\phi}_k, kT_s \leqslant t < (k+1)T_s \tag{5.1}$$

with

$$\eta(t, \boldsymbol{C}_k, \alpha_k) \triangleq 2\pi h \sum_{i=k-L+1}^{k} \alpha_i q(t - iT_s) \tag{5.2}$$

$$\boldsymbol{C}_k \triangleq (\alpha_{k-L+1}, ..., \alpha_{k-2}, \alpha_{k-1}) \tag{5.3}$$

and

$$\boldsymbol{\phi}_k \triangleq \pi h \sum_{i=0}^{k-L} \alpha_i \mod 2\pi. \tag{5.4}$$

In the above equations $\boldsymbol{C}_k$ is the *correlative state*, α_k is the *current symbol*, and $\boldsymbol{\phi}_k$ is the *phase state* of the modulator.

In order to obtain the sampled MF outputs, we assume for the moment that τ is known. The MF outputs are sampled at $\tau + (k+1)T_s$ to produce

$$\boldsymbol{Z}_k(\boldsymbol{C}_k, \alpha_k, \tau) \triangleq \int_{\tau+kT_s}^{\tau+(k+1)T_s} r(t) e^{-j\eta(t-\tau, \boldsymbol{C}_k, \alpha_k)} dt. \tag{5.5}$$

The likelihood function of the data is maximized by performing maximum likelihood sequence detection (MLSD), which is implemented efficiently via the VA. The sampled MF outputs $\boldsymbol{Z}_k$ are used to compute the branch metrics within the VA. The trellis of an SOQPSK modulated signal is shown in Fig. 5.1. The state variables in the trellis are taken from (3.11), and are ordered (u_{k-2}, u_{k-1}) for k-even and (u_{k-1}, u_{k-2}) for k-odd [19]; thus, the trellis states are $S_n \in \{(-1,-1), (-1,+1), (+1,-1), (+1,+1)\}$. The branches in Fig. 5.1 are labeled with the current-bit/current-symbol pair, u_k/α_k, for the given branch. The time-varying nature of the trellis is a result of the time-dependence in (3.11). The remainder of the details needed to implement the VA are found in [16].

In order to obtain the TED update, we temporarily assume that $\boldsymbol{\alpha}$ is known. Using the above definitions, and denoting the observation interval as $0 \le t \le L_0 T$, it can be shown that the likelihood function for the unknown parameter $\tilde{\tau}$ is

$$\Lambda(\boldsymbol{r}|\tilde{\tau}) = \exp\left\{ \frac{1}{N_0} \sqrt{\frac{E_s}{T_s}} \sum_{k=0}^{L_0-1} \text{Re}\left\{ \boldsymbol{Z}_k(\boldsymbol{C}_k, \alpha_k, \tilde{\tau}) e^{-j\phi_k} \right\} \right\}. \tag{5.6}$$

The maximum of $\Lambda(\boldsymbol{r}|\tilde{\tau})$ with respect to the timing offset estimate $\tilde{\tau}$ is obtained by setting equal to zero the partial derivative of (5.6) with respect to $\tilde{\tau}$. Thus, we now have

$$\sum_{k=0}^{L_0-1} \text{Re}\left\{ \boldsymbol{Y}_k(\boldsymbol{C}_k, \alpha_k, \tilde{\tau}) e^{-j\phi_k} \right\} = 0 \tag{5.7}$$

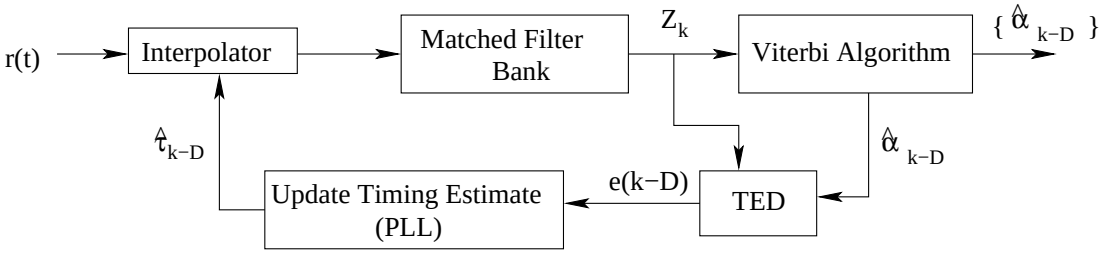

Figure 5.2. Block diagram of the final TED.

where $\boldsymbol{Y}_k$ is the derivative of $\boldsymbol{Z}_k$ with respect to $\tilde{\tau}$. A discrete-time differentiator is used to implement $\boldsymbol{Y}_k$, as discussed in Section 6.2.

The solution to (5.7) is obtained in an adaptive/iterative manner. As it is formulated, (5.7) assumes the true data sequence $\{..., \alpha_{k-2}, \alpha_{k-1}, \alpha_k\}$ is known, which is not the case in practice. A logical substitute for the true data sequence is the sequence of survivors within the VA, which become more reliable the further we trace back along the trellis. Considering all these issues, the following error signal is obtained as in [12]

$$e(k-D) \triangleq \text{Re}\left\{\boldsymbol{Y}_{k-D}(\boldsymbol{C}^b_{k-D}, \alpha^b_{k-D}, \hat{\tau}_{k-D})e^{-j\phi^b_{k-D}}\right\} \tag{5.8}$$

where D is the traceback time for computing the error and the superscript b represents the best survivors of the VA. A large D could result in longer delays in the timing recovery loop, but it is observed in [12] and Section 6.2 that $D = 1T_s$ produces satisfactory results that are discussed in detail in Chap. 6.

A discrete-time implementation of (5.8) is shown in block diagram form in Fig. 5.2.

5.2 S-curve of the TED

The S-curve as explained in 4 helps identify the stable lock points for the TED; these are the zero-crossing points on the curve where the slope is positive, e.g. [11]. In

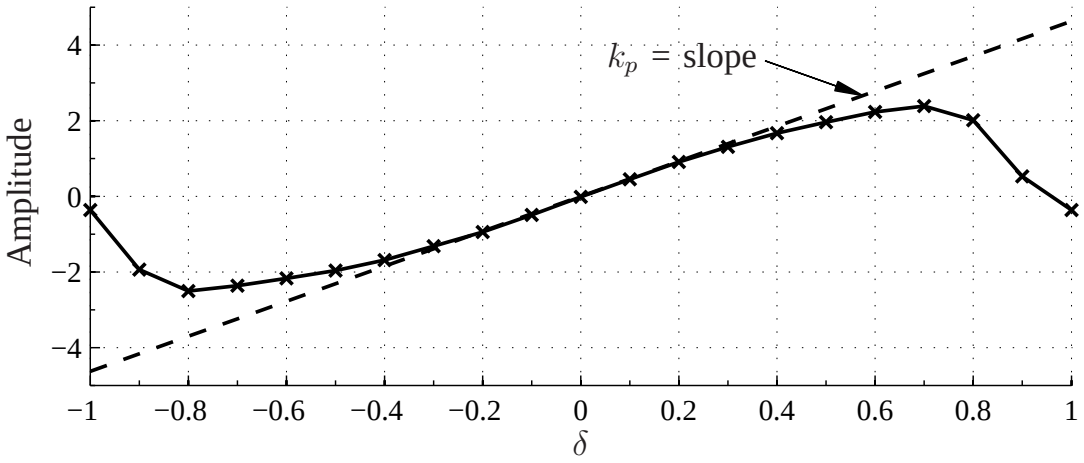

Figure 5.3. S-curve for MIL-STD SOQPSK

this case, a closed-form expression for the expected value of $e[k]$ is rather diffiucult to compute unlike the non-data-aided scheme as the TED is incorporated into the Viterbi algorithm. Hence we use simulations to study the S-curve. The simulations reveal that the only stable lock point occurs when the timing is correct, i.e. at $\delta = 0$. This result holds for both versions of SOQPSK and rules out the existence of false-lock points. The constant k_p is defined as the slope of the S-curve evaluated at $\delta = 0$ and the value of k_p is determined numerically via simulation. The values of k_p determined numerically agree with the values given in [11].

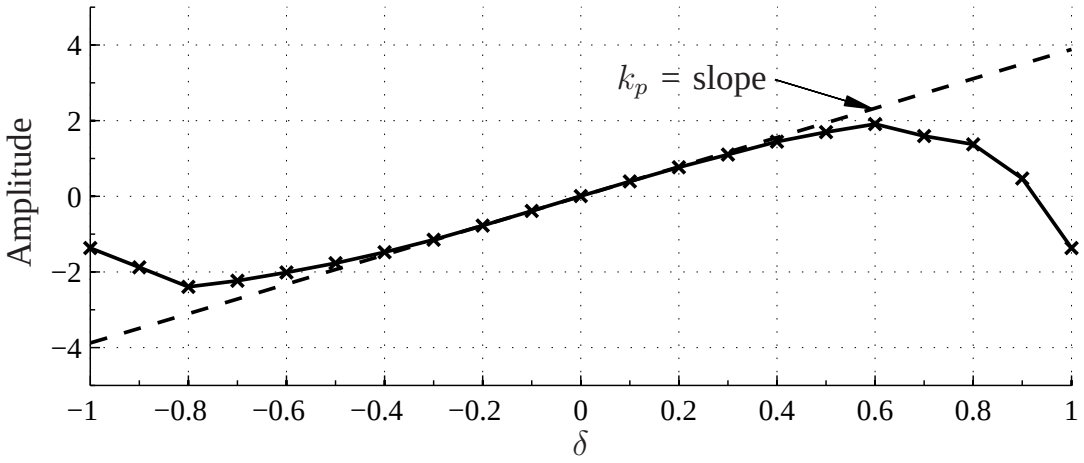

Figure 5.4. S-curve for SOQPSK-TG.

Chapter 6

Numerical Results

In this chapter, we discuss the numerical results obtained by computer simulations for the blind and data-aided TED. The raw TED output $e[k]$ is refined into a more stable timing estimate $\hat{\tau}$ using a feedback scheme. A standard first-order phase-locked loop (PLL) provides an updated timing estimate after each symbol time with the operation

$$\hat{\tau}[k] \triangleq \hat{\tau}[k-1] + \gamma e[k]$$

where the *step size* is

$$\gamma \triangleq \frac{4BT_s}{k_p} \tag{6.1}$$

and BT_s is the user-specified *normalized loop bandwidth*.

The constant k_p is obtained from the S-curve of the TED; this curve characterizes the overall behavior of the TED and is the expected value of the TED output $e[k]$ as a function of the *timing offset*

$$\delta \triangleq \tau - \hat{\tau}.$$

Both TEDs were tested for two loop bandwidths of $BT_s = 10^{-3}$ and $BT_s = 10^{-2}$,

the simulation results of which are explained in the following sections.

We now quantify the accuracy of the TED in Fig. 4.2 for MIL-STD SOQPSK. The raw TED output is refined into a more stable timing estimate $\hat{\tau}$ using a feedback scheme. A standard first-order phase-locked loop (PLL) provides an updated timing estimate after each symbol time with the operation explained in (6.1). The relationship between the observation interval L_0 in a feedforward-based scheme and the normalized loop bandwidth BT_s in a feedback-based scheme is [11]

$$L_0 T_s = \frac{1}{2BT_s}.$$

The accuracy of the feedback scheme is measured with the *normalized timing variance*

$$\frac{1}{T_s^2} \times \sigma_\tau^2 \triangleq \frac{1}{T_s^2} \times \text{Var}\left\{\hat{\tau}[n] - \tau\right\}. \tag{6.2}$$

6.1 Numerical Results for non data-aided TED

We have discussed two cases using loop bandwidths $BT_s = 1 \times 10^{-3}$ and $BT_s = 1 \times 10^{-2}$. With $BT_s = 1 \times 10^{-3}$ all the four filter responses plotted in Figs. 4.1 and 4.3 have been tested. For $BT_s = 1 \times 10^{-2}$, simulation results are provided using the filter response $h_1[k]$. The normalized timing variances for for all these options, each using $N = 4$ are shown in Fig. 6.1, along with the MCRB(τ) in (3.23). Using $BT_s = 1 \times 10^{-3}$, the first observation from Fig. 6.1 is that the filter response $h_1[k]$ clearly outperforms $f_1[k]$, both with and without quantization. This emphasizes that the data correlation can and *should* be taken into account when computing (4.7), which is one of the primary contributions of this work. The second observation from Fig. 6.1 is that the two level quantization scheme $h[k] = Q_1(h_1[k])$ has a negligibly small effect

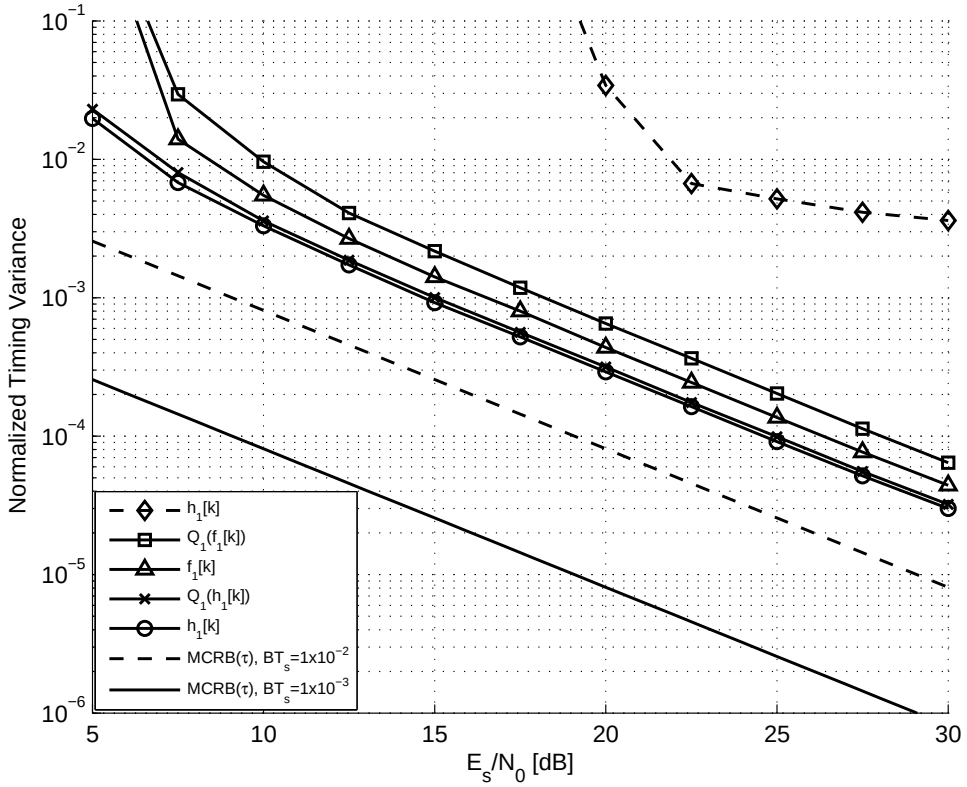

Figure 6.1. MCRB vs. normalized timing variance for MIL-STD SO-QPSK with $N = 4$. Solid curves are for $BT_s = 1 \times 10^{-3}$ and dashed curves are for $BT_s = 1 \times 10^{-2}$.

on the variance of the timing estimate. This is rather pleasing since $h[k] = Q_1(h_1[k])$ reduces the complexity of the TED considerably by a factor as explained in 4.1.3. The last observation for this case from Fig. 6.1 is that the tracking accuracy of the TED in Fig. 4.2 is significantly worse by 15 dB than the performance limit indicated by the MCRB(τ). Using $BT_s = 1 \times 10^{-2}$, the performance of the TED is worse than what was observed with $BT_s = 1 \times 10^{-3}$ in terms of normalized timing variance vs. MCRB. The accuracy in this case is so bad that performance of the TED is rather poor which can be seen in its BER performance shown in Fig. 6.3. This is a drawback with the proposed scheme, but not an unexpected result based on similar findings reported

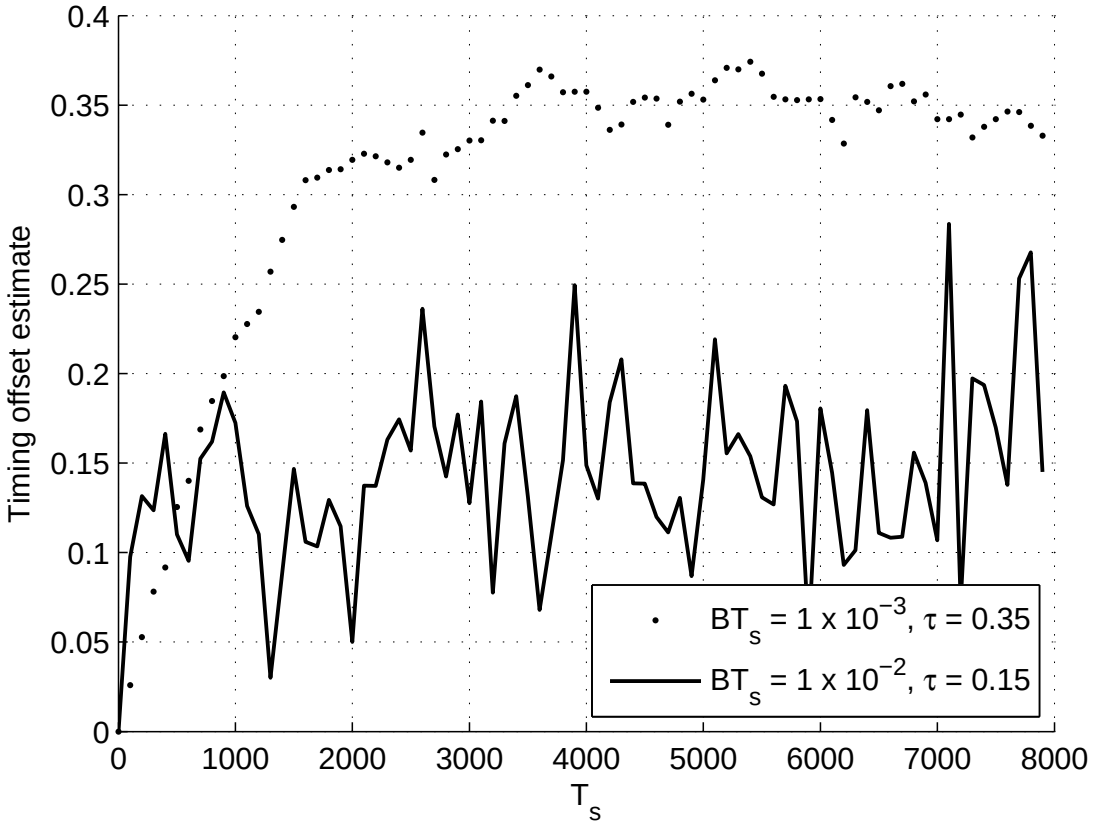

Figure 6.2. Acquisition time of the NDA-TED with a random timing offset

in [5]. However, we emphasize that the proposed scheme has other compelling merits, such as low complexity, no false lock points, and compatibility with a wide range of applications, such as noncoherent detectors.

Fig. 6.2 shows the acquisition time of the TED for the two different loop bandwidths. With $BT_s = 1 \times 10^{-3}$, it can be seen that the TED locks on to the correct timing at around $3500T_s$. But the fact that its performance in terms of normalized timing variance vs. MCRB was rather poor being off from the lower bound by 15 dB is clearly evident here in the form of the jitter in the curve. In case of $BT_s = 1 \times 10^{-2}$, the TED never really locks on to the correct timing and this is an expected result with the normalized timing variance being too high compared to the MCRB, the effect of which

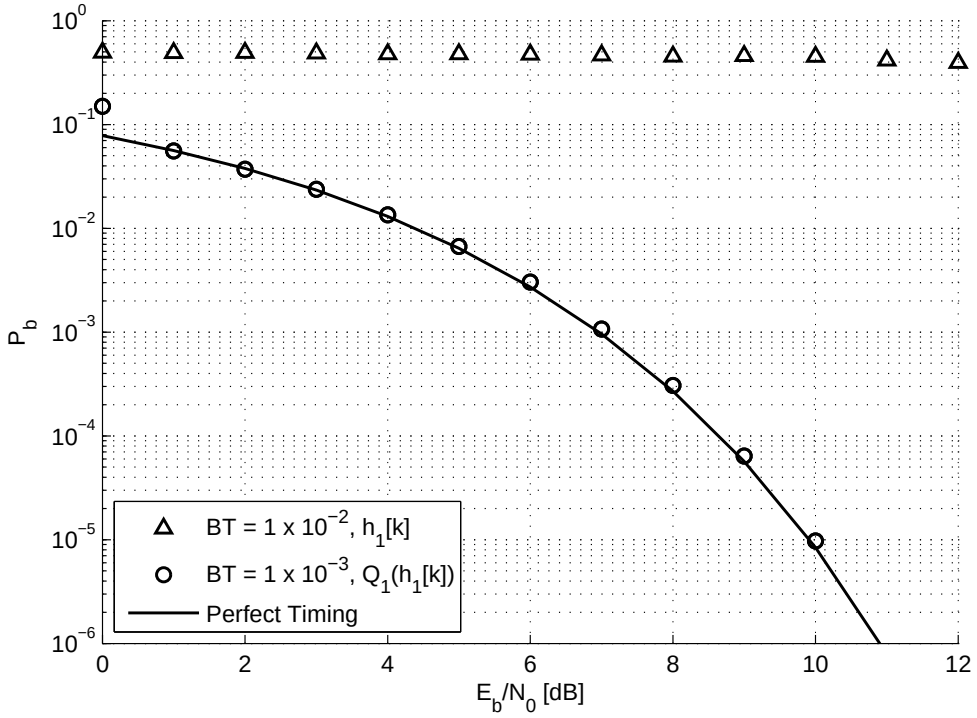

Figure 6.3. Probability of bit error for MIL-STD SOQPSK

can also be seen in the BER performance shown in Fig. 6.3.

Fig. 6.3 quantifies the bit error performance of a MIL-STD SOQPSK detector whose timing estimate comes from the feedback-based timing recovery scheme discussed above. The theoretical performance of the optimal MIL-STD SOQPSK detector with perfect symbol timing is given in [15]. This ideal performance curve is shown in Fig. 6.3 along with the simulated bit error performance of the detector with $BT_s = 1 \times 10^{-3}$ and $h[k] = Q_1(h_1[k])$. The BER performance of the system with $BT_s = 1 \times 10^{-2}$ and $h[k]$ is also shown for the sake of comparison. The detector with $BT_s = 1 \times 10^{-3}$ achieves near-optimal performance for $E_b/N_0 \geq 1$ dB. In fact, the loss due to the imperfect timing estimates is only 0.05 dB at $P_b = 10^{-5}$. This demonstrates the usefulness of the proposed scheme, in spite of the suboptimal tracking performance

shown in Fig. 6.1.

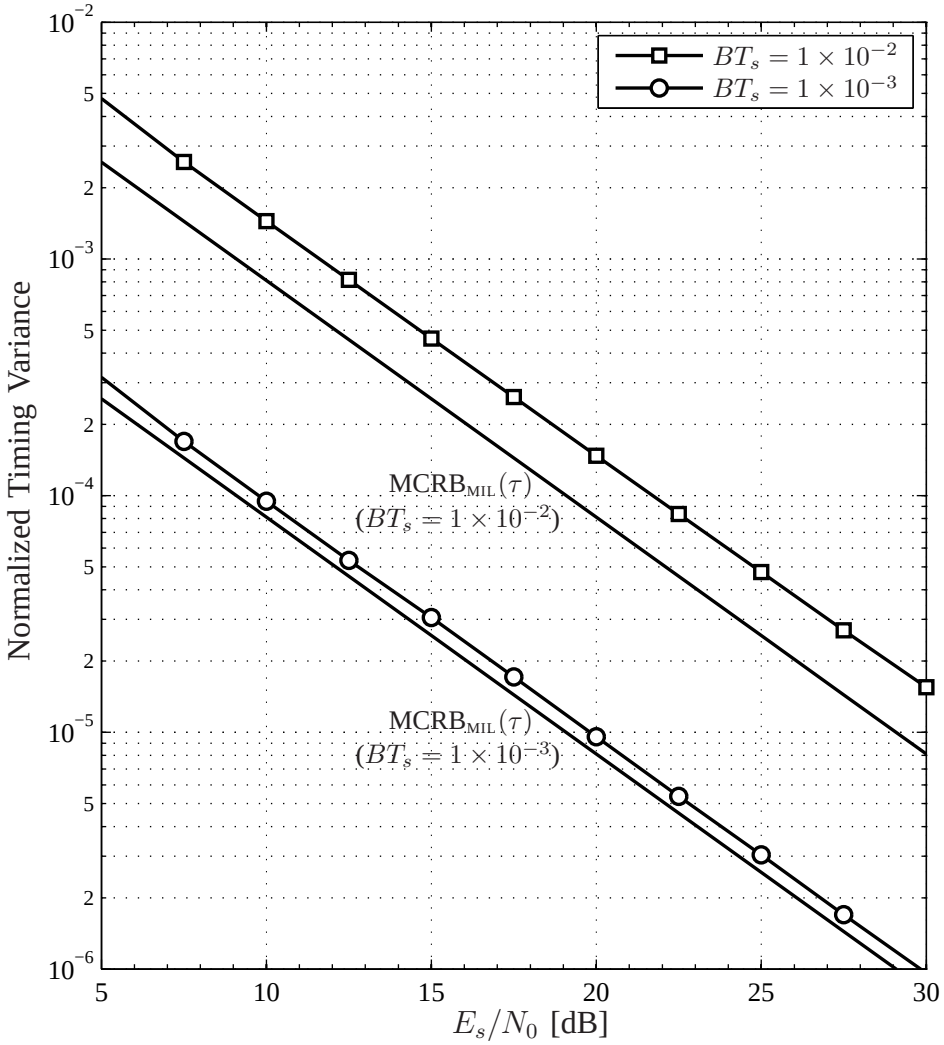

Figure 6.4. MCRB vs. normalized timing variance for MIL-STD SOQPSK with $N = 4$.

6.2 Numerical Results for data-aided TED

The accuracy of the TED in Fig. 5.2 is quantified for the two versions of SOQPSK as it was done for the non-data-aided TED. The discrete-time implementation is sampled at a rate of $N = 4$ samples per symbol. Samples of $\boldsymbol{Z}_k$ are used to update the branch

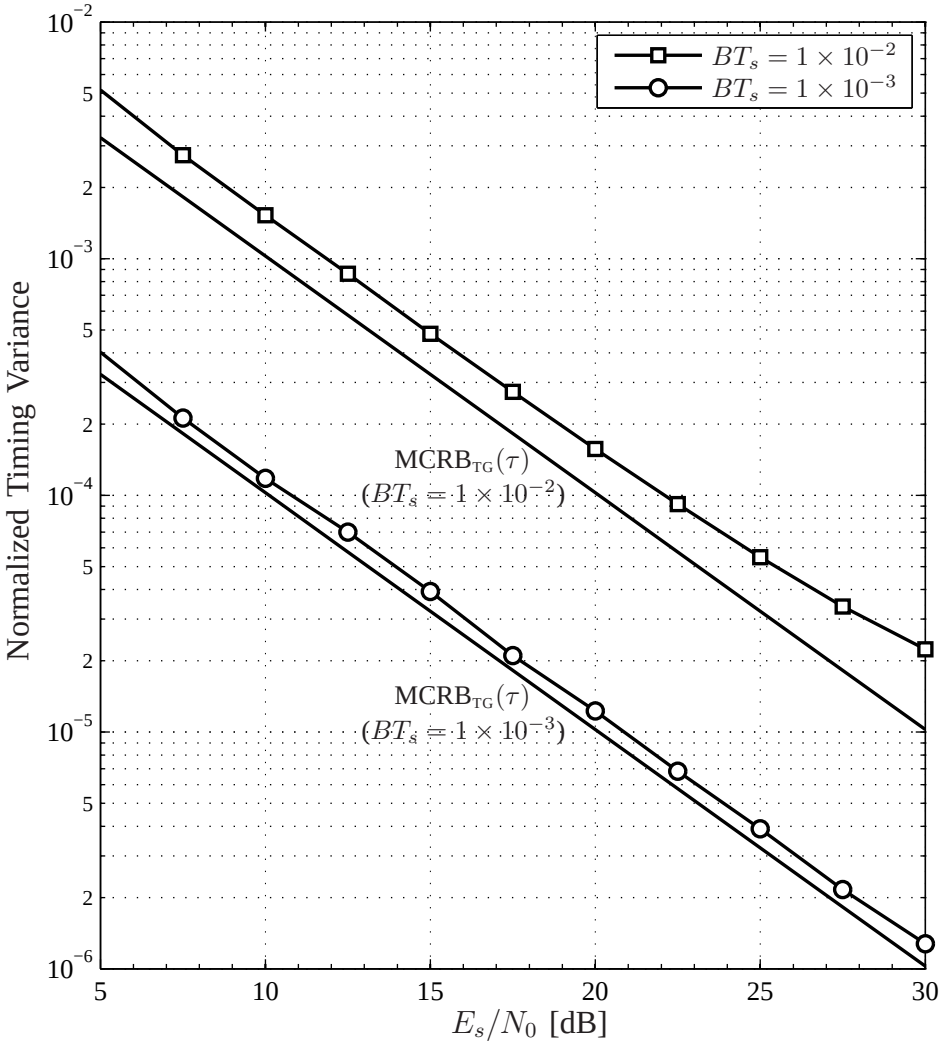

Figure 6.5. MCRB vs. normalized timing variance for SOQPSK-TG with $N = 4$.

metrics within the VA. In addition to the sample used in the VA, an *early* sample of $\boldsymbol{Z}_k$ is taken, as well as a *late* sample. The difference between the early and late samples is used to approximate the derivative $\boldsymbol{Y}_k$. This procedure is discussed in [12].

In this work, the timing variance has been computed for two different values of the normalized loop bandwidth, for both versions of SOQPSK (a total of four cases). Figs. 6.4 and 6.5 show the normalized timing variances plotted along with their corresponding MCRB(τ)'s. All four cases reveal that the TED is very effective for SOQPSK,

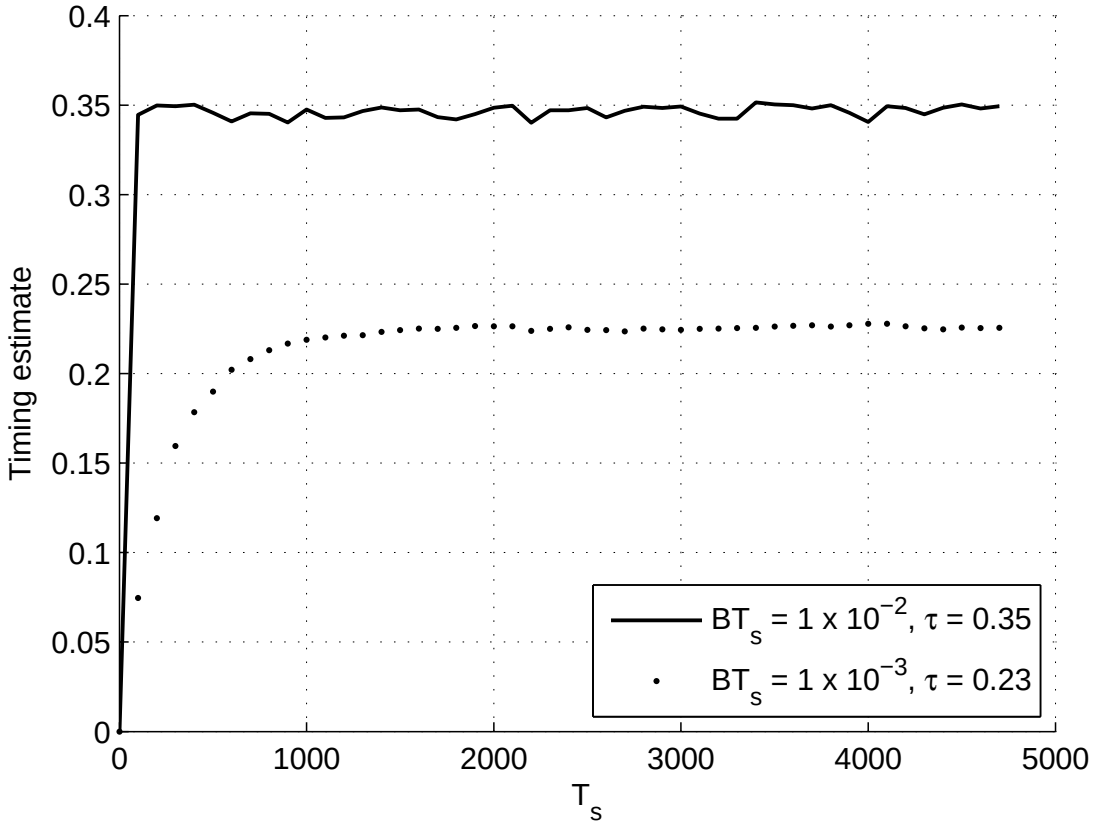

Figure 6.6. Acquisition time of the DA-TED with a random timing offset

since the normalized timing variance is within 2.5dB of the lower performance limit indicated by MCRB(τ).

These synchronization results further validate the CPM model for SOQPSK, which has already proven effective in detection algorithms. Moreover, in the case of SOQPSK-TG where the reduced-complexity pulse truncation approximation is used, it is pleasing that such low values of the timing variance are achieved using the suboptimal MF output samples. The proposed TED shows a marked improvement in performance when compared to the *non data aided* TED developed in Chap. 4. In particular, the TED presented here allows for much wider loop bandwidths and the rapid synchronization times that result. The acquisition time for this TED is shown in 6.6. It is seen that the

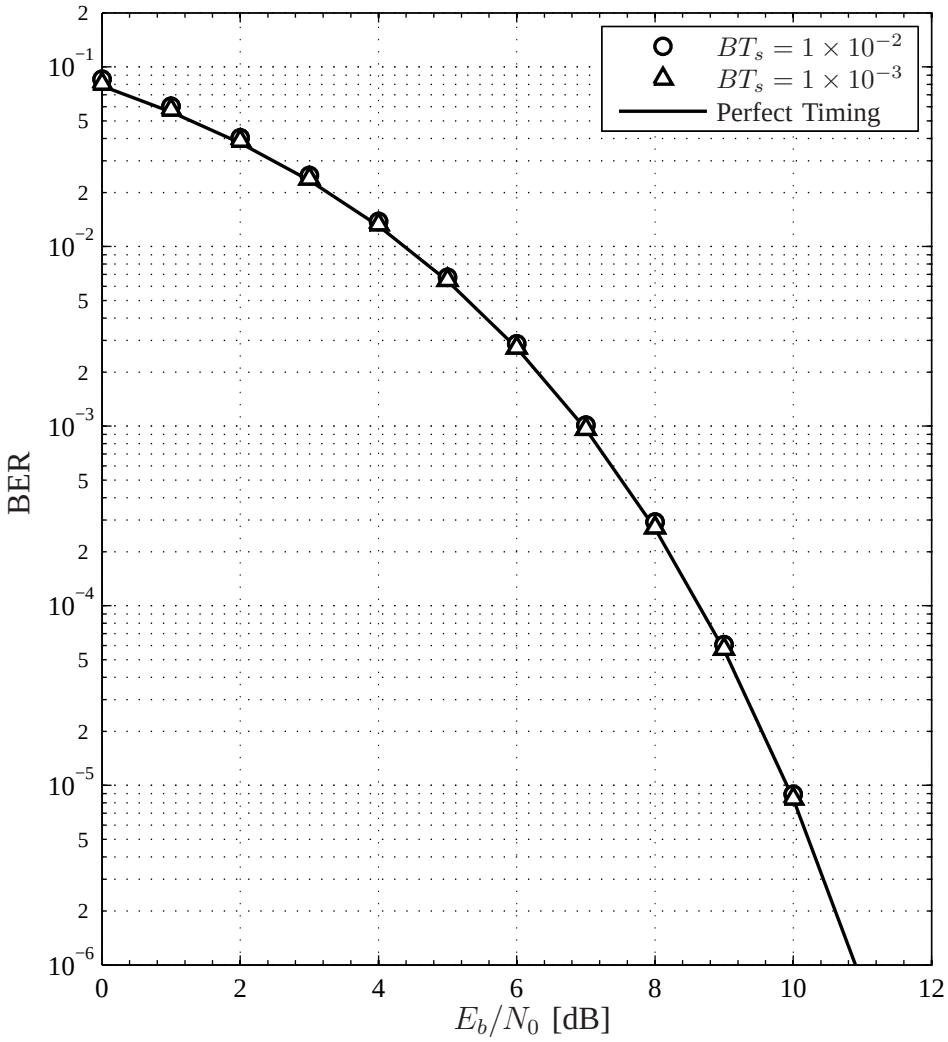

Figure 6.7. Probability of bit error for MIL-STD SOQPSK with $N = 4$.

TED locks on to the correct timing in just over $1000T_s$ when $BT_s = 1 \times 10^{-3}$. When a wider loop bandwidth of $BT_s = 1 \times 10^{-2}$ is used the synchronization time is even faster with the TED locking onto the correct timing as fast as $200T_s$. This is one of the advantages of this TED over its non-data-aided counterpart which failed to synchronize with the correct timing value at this loop bandwidth.

Figs. 6.7 and 6.8 quantify the bit error rate (BER) performances of the proposed TED for MIL-STD SOQPSK and SOQPSK-TG. The theoretical performance of the

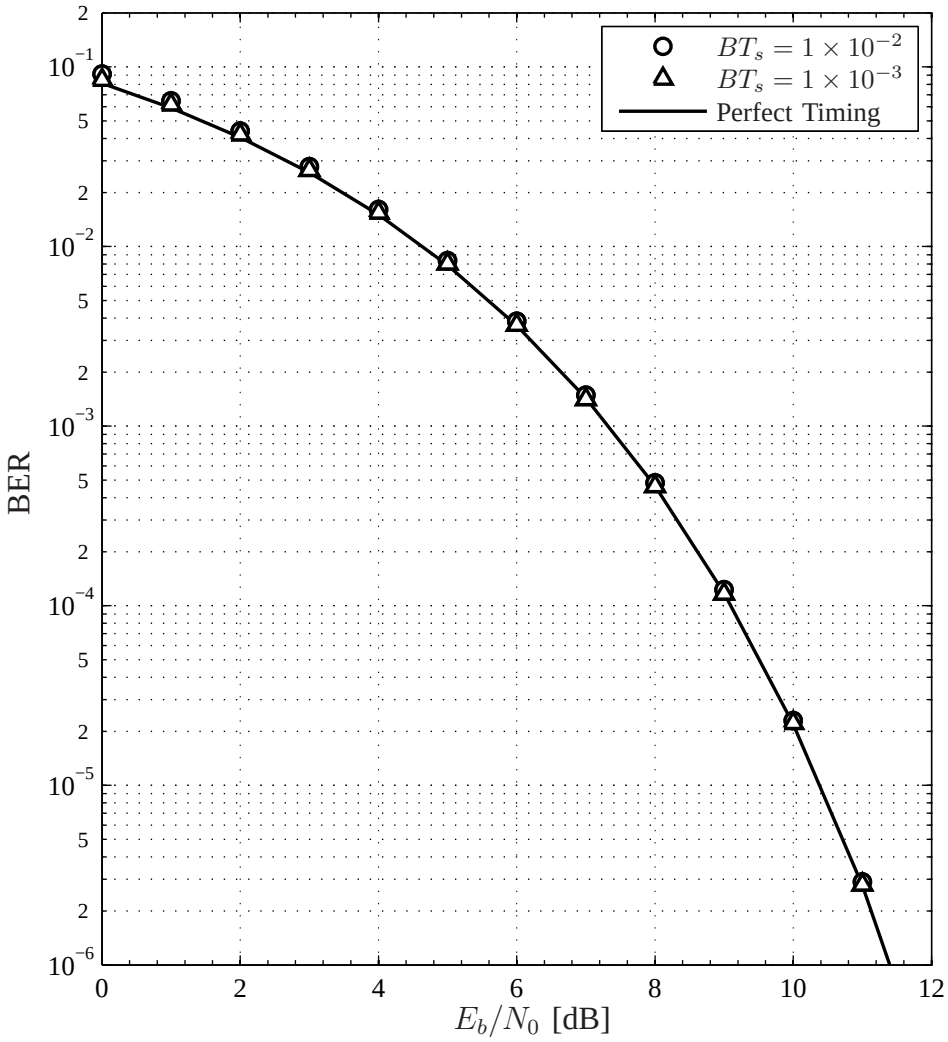

Figure 6.8. Probability of bit error for SOQPSK-TG with $N = 4$.

optimal MIL-STD SOQPSK detector with perfect symbol timing is given in [15]. This ideal performance curve is shown in Fig. 6.7 along with the simulated results for the bit error performance of the TED with $BT_s = 1 \times 10^{-3}$ and $BT_s = 1 \times 10^{-2}$. It can be seen that the detector performs at the theoretical limit, with the simulation points perfectly lining up over the analytical curve. The fact that this performance is achieved with the wider loop bandwidth of $BT_s = 1 \times 10^{-2}$ is noteworthy.

Similarly, the theoretical performance of SOQPSK-TG with the 4-state pulse trun-

cation approximation and perfect symbol timing is given in [16]. As in the previous case, the TED provides accurate results even with $BT_s = 1 \times 10^{-2}$. This demonstrates the applicability of the TED to both versions of SOQPSK, which is significant since the *non data-aided* TED has extremely poor performance in the case of SOQPSK-TG.

Chapter 7

Conclusion

It is clear that synchronization is a very important problem to be addressed in any communication system. SOQPSK with its constrained data symbols does not simplify the task in any way with synchronizers available for CPM's not always being compatible here. Hence reduced-complexity detectors are required. These timing recovery schemes are of practical significance since SOQPSK is widely used in military and aeronautical telemetry. Moreover, CPM-based detectors have only recently been proposed for SOPQSK and compatible timing recovery schemes, such as the ones proposed here, are required for these detectors to be implemented in practice.

In this work, two different types of TED's compatible with SOQPSK have been proposed namely the non-data-aided (blind) TED and the data aided TED. Both the TED's have their respective merits and demerits. Considering the blind TED it has been shown that the data correlation can be ignored when constructing the TED; however, the best results are obtained when the data correlation is taken into account. The S-curve of the TED was computed, which ruled out the existence of false lock points. In the case of SOQPSK, the proposed scheme was shown to have relatively poor performance by 15 dB in terms of timing error variance, as measured against the MCRB. However,

due to its simplicity, its blind nature, and the absence of false lock points, the proposed scheme has potential in a wide range of applications and is an attractive solution to this highly-motivated problem.

As far as the data aided TED is concerned, unlike the other TED, the performance is exceptionally good in terms of approaching the theoretical lower bounds on timing error variance established by the MCRB. Furthermore, the bit error performance of the detector was identical to the perfect timing case, even when reasonably large values of the loop bandwidth were used.

Though the performance of the data aided TED is superior in terms of normalized variance, the blind TED has its own advantages. In applications where interaction between phase and timing is not desirable, the blind TED is the only solution available today. Moreover, the performance of the blind TED is comparable to the data aided TED considering the BER's of the two schemes. It is particularly pleasing to note that a drastically simplified two level quantized blind TED performed close to the theoretical limit.

Acknowledgment

This work was supported by the T&E/S&T Test Resource Management Center (TRMC) through the White Sands Contracting Office, contract number W9124Q-06-P-0337.

References

[1] D. I. S. Agency. Department of Defense interface standard, interoperability standard for single-access 5-kHz and 25-kHz UHF satellite communications channels. Tech. Rep. MIL-STD-188-181B, Department of Defense, Mar. 1999.

[2] J. B. Anderson, T. Aulin, and C.-E. Sundberg. *Digital Phase Modulation*. Plenum Press, New York, 1986.

[3] T. Aulin, C.-E. Sundberg, and A. Svensson. Viterbi detectors with reduced complexity for partial response continuous phase modulation. In *Proc. National Telecommun. Conf., NTC'81*, pages A7.6.1–A7.6.7, New Orleans, LA, Nov./Dec. 1981.

[4] G. Colavolpe and R. Raheli. Noncoherent sequence detection of continuous phase modulations. *IEEE Trans. Commun.*, 47(9):1303–1307, Sep. 1999.

[5] A. N. D'Andrea, U. Mengali, and M. Morelli. Symbol timing estimation with CPM modulation. *IEEE Trans. Commun.*, 44(10):1362–1372, Oct. 1996.

[6] A. N. D'Andrea, U. Mengali, and R. Reggiannini. The modified Cramer-Rao bound and its application to synchronization problems. *IEEE Trans. Commun.*, 42(2/3/4):1391–1399, Feb./Mar./Apr. 1994.

[7] M. J. Dapper and T. J. Hill. SBPSK: A robust bandwidth-efficient modulation for hard-limited channels. In *Proc. IEEE Military Commun. Conf.*, Oct. 1984.

[8] T. Hill. A non-proprietary, constant envelope, variant of shaped offset QPSK (SOQPSK) for improved spectral containment and detection efficiency. In *Proc. IEEE Military Commun. Conf.*, Oct. 2000.

[9] P. A. Laurent. Exact and approximate construction of digital phase modulations by superposition of amplitude modulated pulses (AMP). *IEEE Trans. Commun.*, 34(2):150–160, Feb. 1986.

[10] L. Li and M. Simon. Performance of coded OQPSK and MIL-STD SOQPSK with iterative decoding. *IEEE Trans. Commun.*, 52(11):1890–1900, Nov. 2004.

[11] U. Mengali and A. N. D'Andrea. *Synchronization Techniques for Digital Receivers*. Plenum Press, New York, 1997.

[12] M. Morelli, U. Mengali, and G. M. Vitetta. Joint phase and timing recovery with CPM signals. *IEEE Trans. Commun.*, 45(7):867–876, Jul. 1997.

[13] T. Nelson, E. Perrins, and M. Rice. Common detectors for shaped offset QPSK (SOQPSK) and Feher-patented QPSK (FQPSK). In *Proc. IEEE Global Telecommun. Conf.*, Nov./Dec. 2005.

[14] E. Perrins and M. Rice. PAM representation of ternary CPM. to be published in *IEEE Trans. Commun.*

[15] E. Perrins and M. Rice. Simple detectors for shaped-offset QPSK using the PAM decomposition. In *Proc. IEEE Global Telecommun. Conf.*, pages 408–412, St. Louis, Missouri, Nov./Dec. 2005.

[16] E. Perrins and M. Rice. Reduced-complexity approach to iterative detection of SOQPSK. *IEEE Trans. Commun.*, 55(7):1354–1362, Jul. 2007.

[17] E. Perrins, R. Schober, M. Rice, and M. K. Simon. Multiple-bit differential detection of shaped-offset QPSK. *IEEE Trans. Commun.*, 55(12):2328–2340, Dec. 2007.

[18] Range Commanders Council Telemetry Group, Range Commanders Council, White Sands Missile Range, New Mexico. *IRIG Standard 106-04: Telemetry Standards*, 2004. (Available on-line at http://www.ntia.doc.gov/osmhome/106.pdf).

[19] M. Simon. *Bandwidth-Efficient Digital Modulation With Application to Deep-Space Communication*. Wiley, New York, 2003.

[20] M. K. Simon. Multiple-bit differential detection of offset QPSK. *IEEE Trans. Commun.*, 51(6):1004–1011, Jun. 2003.

[21] A. Svensson, C.-E. Sundberg, and T. Aulin. A class of reduced-complexity Viterbi detectors for partial response continuous phase modulation. *IEEE Trans. Commun.*, 32(10):1079–1087, Oct. 1984.